Planar assembly of monodisperse metallic cobalt nanoparticles embedded in $TiO_{2-\delta}$ matrix

2007 J. Phys.: Condens. Matter 19 116205

(http://iopscience.iop.org/0953-8984/19/11/116205)

IOP PUBLISHING JOURNAL OF PHYSICS: CONDENSED MATTER

J. Phys.: Condens. Matter **19** (2007) 116205 (8pp) doi:10.1088/0953-8984/19/11/116205

Planar assembly of monodisperse metallic cobalt nanoparticles embedded in $TiO_{2-\delta}$ matrix

B Vodungbo[1], Y Zheng[1], M Marangolo[1], D Demaille[1] and J Varalda[2]

[1] Institut des Nanosciences de Paris, UMR 7588 CNRS—Universités Pierre et Marie Curie et Denis Diderot, Campus Boucicaut, 140 rue de Lourmel, 75015 Paris, France
[2] Departamento de Física—UFSCar, CP 676, 13565-905 São Carlos SP, Brazil

E-mail: boris.vodungbo@insp.jussieu.fr

Received 13 December 2006, in final form 30 January 2007
Published 5 March 2007
Online at stacks.iop.org/JPhysCM/19/116205

Abstract

We report the growth of a single layer of metallic cobalt nanoparticles in a $TiO_{2-\delta}$ matrix. The films are grown by pulsed laser deposition (PLD). Transmission electron microscopy (TEM) is used to determine the morphology of the system and the crystalline structure (HCP and/or FCC) of the cobalt nanoparticles. A sharp interface between the nanoparticles and the matrix is observed. Electron energy loss spectroscopy (EELS) is used to investigate the metallic character of the cobalt. Oxidation of cobalt at the interface with the matrix is not observed. With regards to the importance of the matrix for transport properties and because of the great variability of the oxygen content of $TiO_{2-\delta}$, efforts were also made on the analysis of $TiO_{2-\delta}$ matrix. EELS measurements indicate an oxygen deficiency with respect to the nominal TiO_2 composition which increases with growth temperature. This leads to a rather low resistivity of the matrix which also decreases with increasing growth temperature.

1. Introduction

In recent decades, nanosized multilayers or granular systems including magnetic metal such as cobalt, iron or nickel have been intensively studied. This led to the discovery of giant magnetoresistance (GMR) in iron chromium multilayers in 1988 [1] and a few years later in systems made of cobalt nanoparticles embedded in a metallic matrix such as copper or silver [2, 3]. Since then a lot of work has been done to enhance the GMR in granular cobalt systems and to understand its origins, both theoretically and experimentally [4–6].

In the same time, granular cobalt systems based on an insulating matrix such as Al_2O_3, SiO_2, CoO, ZrO_2 and inert gas were found to exhibit tunnelling magnetoresistance (TMR) [7–11]. In fact, in magnetic granular systems TMR was already observed long ago in Ni–SiO_2 and Co–SiO_2 [12, 13], but the discovery of GMR has stimulated the study of TMR in these systems. In magnetic granular metals the magnetoresistance is due to the spin-dependent

tunnelling of the conduction electron: the tunnelling probability of an electron with spin parallel to the particle magnetization is higher than that of one with antiparallel spin. Thus the resistance decreases when the particles' magnetic moments align in response to a magnetic field.

The models of TMR developed by Helman and Abeles [14] and by Inoue and Maekawa [15] were able to reproduce the main observed temperature dependence of TMR. The first one shows a T^{-1} temperature dependence of the TMR whereas, for the second, the TMR is nearly temperature independent over a wide temperature range. Both models fail to explain the large TMR increase sometimes observed at very low temperature [16]. Mitani and co-workers extended the Inoue and Maekawa model to take into account tunnelling between granules of different sizes [16]. They claimed that the large TMR increase at low temperature needed higher-order tunnelling processes, i.e. tunnelling processes involving more than two nanoparticles. This feature is supposed to be inherent to granular systems with a broad particle size distribution although it has also been observed in rather monodisperse granular systems [9, 11].

Recently, the interest in granular systems has been extended to the study of current-induced magnetization reversal (CIMR) where the magnetization of a nanomagnet is reversed not by an external magnetic field but by spin transfer torque from high-density spin-polarized currents. In these studies, both high GMR and TMR were found [5, 17].

The fabrication processes of magnetic granular systems are varied, but co-sputtering or co-evaporation are mostly used [7, 8, 12, 13]. The nanoparticle assemblies obtained by these methods typically show a broad particle size distribution with a correlation between the magnetic metal fraction and the mean particle size. For example, it is difficult to produce an assembly of small particles with low homogeneous interparticle distance. Moreover, magnetic impurities embedded in the insulating matrix are very likely to be present, influencing the spin-dependent tunnelling [19]. Another point which is rarely discussed is the chemical reactivity at the metal/matrix interface. In fact, a high-quality metal/matrix interface is important for maintaining the spin polarization across the structure. But within an oxide matrix, surface oxidation of the magnetic material is highly possible [20, 21]. Such an oxidized shell around the nanoparticles could also influence the spin-dependent tunnelling. An optimum control of sample properties such as nanoparticles size, interparticle distance and metal/matrix interface is then required to understand better and possibly enhance the TMR and CIMR effects. Only a few techniques have been proposed to obtain such well-defined granular systems, for example cluster beam deposition and pulsed laser deposition [9–11].

In this paper, we study the structural properties of a planar assembly of cobalt nanoparticles embedded in a $TiO_{2-\delta}$ matrix. Cobalt is a ferromagnetic metal with high Curie temperature and spin polarization ($P_{Co} = 0.45$). Titanium dioxide is a wide band-gap (3.1 eV) semiconductor, extensively studied for spintronics and optoelectronics applications since 2001 [22]. The structure of the nanoparticles and the cobalt valence state are examined together with some of the matrix properties such as stoichiometry and conductivity. The differences between samples grown at room temperature, 350 °C and 650 °C are also investigated. The magnetic properties and TMR of this system have already been studied and the results have been reported elsewhere. In the low-bias regime, a maximum TMR of about 6% is observed at low temperature [18]. The TMR rapidly decreases with increasing temperature. In the high-bias regime, a very high TMR of about 300% was observed at low temperature [17].

2. Experimental details

A pulsed excimer KrF laser ($\lambda = 248$ nm, $\tau = 20$ ns) was used at a fluence of about 3 J cm^{-2} and a repetition rate of 2 Hz. The distance between the substrate and the target was 5 cm. The

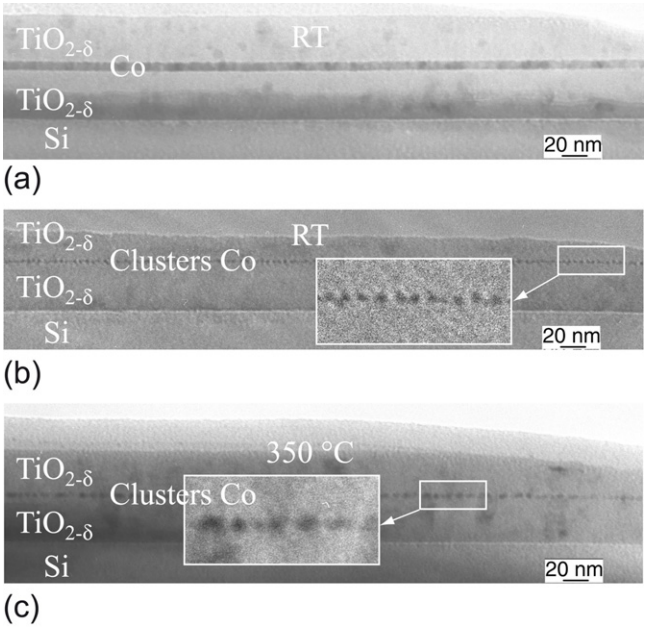

Figure 1. TEM images of cobalt embedded in a $TiO_{2-\delta}$ matrix: (a) 6 nm thick continuous film of cobalt grown at RT, (b) Co clusters layer grown at RT, with an amount of Co equivalent to a 1 nm continuous layer, (c) Co clusters layer grown at 350 °C, with an amount of Co equivalent to a 1 nm continuous layer.

substrate temperature was set either at room temperature (RT), at 350 °C, or at 650 °C. The growth was performed under vacuum (10^{-6} mbar) with metallic Co and nominal TiO_2 targets.

Transmission electron microscopy (TEM) was used to determine the film structure and the crystalline structure of Co clusters. TEM observations were made with a JEM 2100F microscope operating at 200 kV and equipped with a Gatan GIF spectrometer. The valence state of Co and composition of the $TiO_{2-\delta}$ matrix were investigated by electron energy loss spectroscopy (EELS). The conductivity of the $TiO_{2-\delta}$ matrix was measured by the four-point method using evaporated-gold contacts. Optical absorption spectra were recorded with a UV–vis–NIR CARY 500 spectrometer.

3. Results and discussion

3.1. Co film structures

A thick $TiO_{2-\delta}$ buffer layer, typically 40 nm, was first grown on the native thin oxide layer of a Si(100) wafer. Co films were grown on the $TiO_{2-\delta}$ buffer layer, followed by an over-layer of $TiO_{2-\delta}$. Both $TiO_{2-\delta}$ layers are amorphous. Two types of embedded Co films are involved here: a continuous Co film and a single layer of Co clusters (figure 1). Figure 1(a) shows a continuous film of 6 nm thickness grown at RT. TEM observations indicate that the film is polycrystalline with crystal grains of 6 nm in height and of about 10 nm in width. Both the α phase (HCP structure) and β phase (FCC structure) of Co are present, with a predominance of FCC structure (figure 2). Similar films were obtained at 350 °C.

When an amount of Co equivalent to a 1 nm continuous layer is deposited at RT, the growth of Co is stopped at the nucleation stage. Then, small and closely packed clusters are

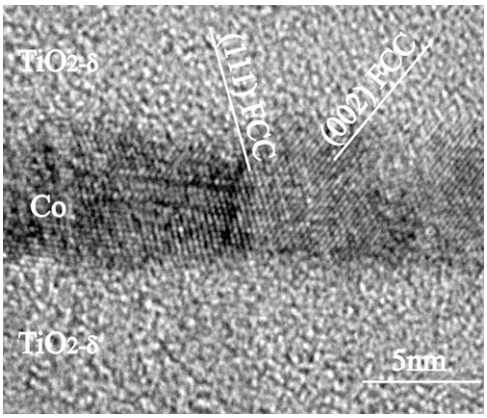

Figure 2. High-resolution TEM (HRTEM) images of a 6 nm thick polycrystalline film of cobalt grown at room temperature.

formed (figure 1(b)). The clusters are quite homogeneous, with a diameter of about 3 nm and a separation distance of about 2 nm. Such single layers of monodisperse clusters exhibit interesting properties in magnetism and tunnel electronic transport [17, 18]. Thus, the nature of the clusters should be clarified. Lattice imaging was unsuccessful inside the clusters in the present case. In fact, contrasts inside such small clusters are too weak compared to those inside matrix. Moreover, amorphous $TiO_{2-\delta}$ matrix crystallizes under the electron beam leading to even more contrasts. The results of the spectroscopic analysis (EELS) undertaken in order to determine the Co valence state in the small clusters are given below.

Similar growth occurs at 350 °C. However, the clusters begin to have an oblate shape, with a height of about 3 nm and a width of about 4 nm. The clusters are less monodisperse than those grown at RT. The separation distance between clusters ranges from 2 to 3 nm.

When the same amount of Co is deposited at high temperature (650 °C), large clusters of Co are formed. Large clusters are of oblate shape with a broad size distribution from 5 to 10 nm. The inter-cluster distance is generally greater than 10 nm. Lattice imaging indicates that the clusters are mostly of FCC structure. Such polydisperse and widely separated clusters are *a priori* not interesting for tunnel magneto-electronic transport.

3.2. Co valence state in small clusters

Co clusters of about 10 nm in diameter, i.e. grown at 650 °C, are of metallic structure, as observed in HRTEM lattice images. If an oxide coating exists, it cannot exceed a few atomic layers. Questions remain for the case of small clusters with about 3 nm diameter or lower. One important point is to clarify the chemical nature of Co in small clusters. Due to the increasing importance of the surface versus the volume in small clusters, an oxide coating could induce a large proportion of non-metallic Co. The nature of clusters and the interface between clusters and matrix are key parameters controlling the tunnel electronic transport between clusters and the magnetic properties of clusters. EELS measurements were made in order to probe the Co valence state. The energy resolution (1 eV) does not permit one to detail the chemical shift between Co^0, Co^{2+} and Co^{3+} at the L edge. However, it is well known that the shapes of the L_3 and L_2 white lines and their intensity ratio are sensitive criteria of the Co valence state [23].

Reference EELS spectra of Co^{2+} and Co^{3+}/Co^{2+} at the L edge were first established from CoO and Co_3O_4 crystals in a powder sample. A Co_3O_4 crystal of about 80 nm diameter was identified with HRTEM lattices images. The EELS reference spectrum of Co^{3+}/Co^{2+} (figure 3) was taken for this crystal in diffraction mode, under similar conditions to those which were

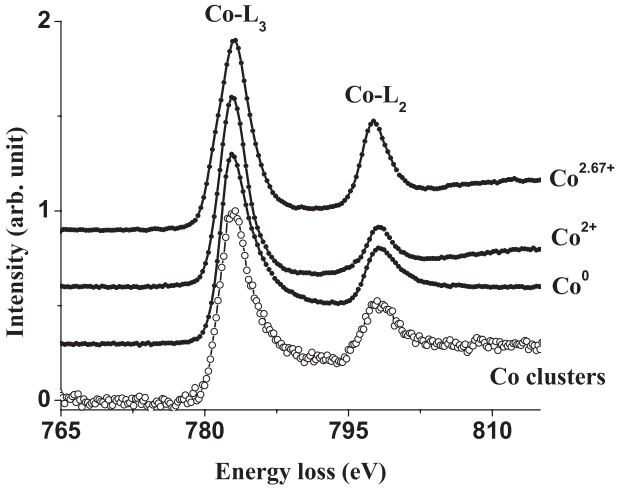

Figure 3. EELS spectra at the Co L edge of cobalt nanoparticles grown at RT embedded in a $TiO_{2-\delta}$ matrix compared to metallic cobalt, CoO and Co_3O_4 references.

used for small Co clusters. The effective Co valence is +2.67 in this case. The spectrum of Co^{2+} was obtained from a crystal of about 70 nm diameter, previously identified as CoO by HRTEM. The spectrum of Co^0 was established with a continuous polycrystalline Co film of 6 nm thickness grown by PLD at RT. A spectrum obtained in Co clusters with 3 nm diameter and grown at RT is displayed in figure 3 with the reference ones. Similar spectra were obtained with small Co clusters grown at 350 °C. The secondary electron background in the spectra was removed and the spectra were normalized for comparison. At this point, it is important to note that the electron beam we use for EELS measurements is rather large ($\gg$10 nm), in order to avoid sample damage. Thus the EELS measurements of Co clusters are not spatially resolved but are recorded from a large number of Co clusters.

In the Co $L_{2,3}$ spectra, one may notice two main features concerning the intensity ratio of L_3/L_2 white lines and the spectrum shape. The intensity ratio of L_3/L_2 white lines in Co clusters and the Co^0 reference is much higher than that in Co_3O_4 ($Co^{2.67+}$) and smaller than that in CoO (Co^{2+}). The shape of L_3 and L_2 white lines is more asymmetric in the case of metallic Co than in the case of cobalt oxides. Beyond the L_3 and L_2 white lines, the background steps in the spectra of Co clusters and Co^0 reference are also higher than those for cobalt oxides. It is obvious for the present case that the spectrum of small clusters is close to the metallic Co one. More precisely, and within the limits of the present EELS technique used, no differences can be observed between the small clusters and metallic Co. The nanoparticles are therefore mainly composed of metallic cobalt.

At this point it is important to recall that the particles are very small. Indeed, for a spherical nanoparticle of 3 nm diameter, surface atoms represent more than 30% of all atoms. If there was a strong charge transfer between oxygen ions of the matrix and the surface cobalt atoms of the nanoparticles, a large amount of cobalt atoms would be oxidized. In this case the EELS spectrum of small clusters would deviate from that of metallic cobalt. This is clearly not observed. The presence of an oxidized shell, equivalent to the oxidation of all the surface Co atoms, can be excluded in our nanoparticles. The interface between the nanoparticles and the matrix is then an abrupt metal/insulator interface.

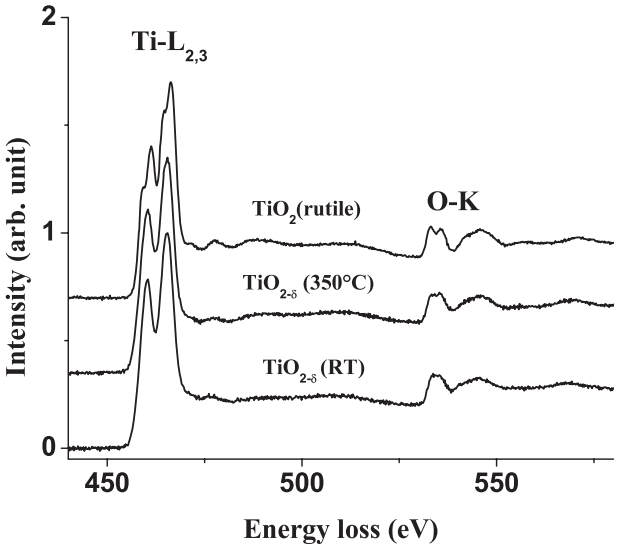

Figure 4. EELS spectra at Ti L and O K edges of $TiO_{2-\delta}$ films grown at RT and 350 °C compared to a rutile reference.

3.3. $TiO_{2-\delta}$ matrix characteristics

It is well known that titanium oxides have a large variability in oxygen stoichiometry, with compositions varying from TiO to TiO_2 [24]. The physical properties are strongly dependent on the oxygen stoichiometry. The chemistry of the $TiO_{2-\delta}$ matrix grown at RT and 350 °C has been investigated by EELS measurements. A EELS reference was first made in a TiO_2 rutile crystal under similar conditions to those which were used for the $TiO_{2-\delta}$ matrix. Figure 4 displays the spectra of the $TiO_{2-\delta}$ matrix grown at RT and 350 °C, together with the rutile reference. For these spectra, the secondary electron background was subtracted. The shapes of the Ti $L_{2,3}$ white lines and the O K edge are quite similar in the amorphous $TiO_{2-\delta}$ matrix and rutile. However, one can notice that the crystalline field of octahedral symmetry in rutile leads to a splitting of the Ti $L_{2,3}$ white lines (and of the O K edge). This disappeared in the amorphous $TiO_{2-\delta}$ matrix, as expected. One should point out that the shapes in EELS spectra are very sensitive to the local atomic environment, especially for O K edge. In particular, EELS spectra of TiO_2 anatase and TiO crystals are different from the rutile one [25]. With respect to the local chemistry, the amorphous $TiO_{2-\delta}$ matrix grown can be qualified as rutile-like. The ratio of the O K edge net area to the Ti L one can be used to provide an estimate of the matrix composition, taking rutile as the standard. As reported in the literature [25], the cross sections of Ti L and O K edges in EELS are structure dependent, and the composition determination cannot be very precise. However, for the present case the similarity in EELS of the $TiO_{2-\delta}$ matrix grown and the rutile crystal allows us to take rutile as the standard and to use the method to establish a composition deviation from rutile. Taking a window of 30 eV over the Ti L and O K edges, the composition is found to be $TiO_{1.95\pm0.05}$ for the matrix grown at RT and $TiO_{1.85\pm0.05}$ for the matrix grown at 350 °C. The results remain stable when the window varies from 20 to 40 eV.

The electronic and electric properties of $TiO_{2-\delta}$ matrix are important features in the magneto-transport in this granular system. In particular, the energy gap of the matrix is an important parameter for determining the barrier height in the tunnel transport process between metallic clusters. Films of $TiO_{2-\delta}$ matrix were grown at RT and 350 °C on silica for optical absorption (120 nm) and electric measurements (60 nm). Although the $TiO_{2-\delta}$ matrices grown

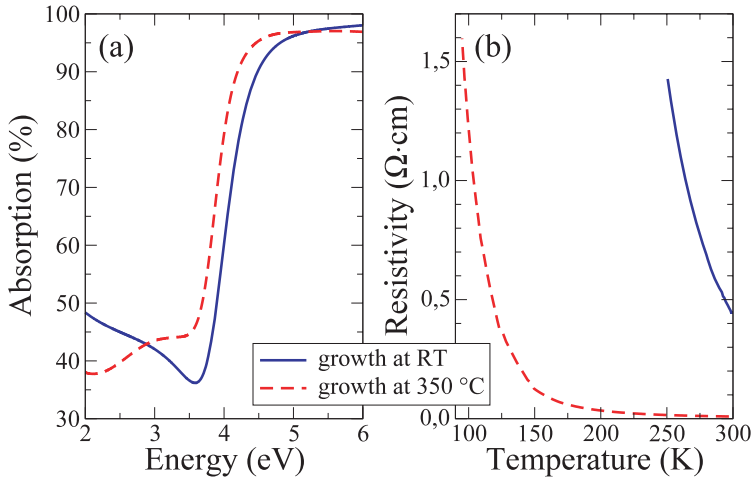

Figure 5. (a) Optical absorption curves of $TiO_{2-\delta}$ films grown at RT and 350 °C. (b) Resistivity versus temperature curves of $TiO_{2-\delta}$ films grown at RT and 350 °C.

(This figure is in colour only in the electronic version)

at RT and 350 °C have compositions close to rutile, their physical properties appear to be quite different, and sensitively depend on the temperature. From optical absorption (figure 5(a)), an apparent optical energy gap of about 2.9 eV for the matrix grown at RT was found using the relation between absorbance and energy for indirect transitions [26]. It is a bit lower than the TiO_2 energy gap in either the rutile (3.0 eV [27]) or anatase (3.2 eV [28]) form. For the matrix grown at 350 °C, the optical energy gap is 2.7 eV, but after a 2 h post-annealing at 350 °C under an O_2 pressure of 1 bar, the gap increases up to 3.0 eV, reaching that of rutile.

Electrical measurements revealed a semiconducting behaviour of the $TiO_{2-\delta}$ matrix (figure 5(b)) with a resistivity of 0.5 Ω cm at RT. Increasing the growth temperature strongly reduces the resistivity of the $TiO_{2-\delta}$ matrix down to 10^{-2} Ω cm. This is consistent with the stoichiometry deduced from EELS data since the resistivity of TiO_2 decreased with increasing concentration of oxygen vacancies [29].

4. Conclusion

Cobalt layers embedded in a $TiO_{2-\delta}$ matrix have been successfully grown at RT and at 350 °C. The structural properties of these layers have been investigated by TEM. For an equivalent amount of cobalt of 6 nm, a continuous layer consisting of polycrystalline metallic cobalt is produced. For an equivalent amount of cobalt of 1 nm deposited at RT, a planar assembly of nanoparticles is produced. In the latter case the mean diameter of the nanoparticles is 3 nm and the interparticle distance is around 2 nm. EELS measurements allowed us to determine that the nanoparticles are mainly composed of metallic cobalt. No oxidized shell could be observed.

The influence of temperature on the morphology of the nanoparticles is small until 350 °C. No differences were detected by EELS between nanoparticles grown at RT and 350 °C. The matrix is much more sensitive to the growth temperature. EELS data show that the oxygen content of the $TiO_{2-\delta}$ matrix decreases with increasing growth temperatures from $2-\delta = 1.95 \pm 0.05$ to $2-\delta = 1.85 \pm 0.05$. The optical gap and the resistivity also decrease with increasing growth temperatures.

The planar assembly of cobalt nanoparticles produced for a low amount of cobalt deposited is very interesting for studying magnetoresitive effects in a granular system. The

nanoparticle size and the interparticle distance are rather uniform compared to the system usually studied. The absence of an oxidized cobalt shell leads to an abrupt metallic cobalt/insulating $TiO_{2-\delta}$ interface. The properties of the matrix can be varied independently from those of the nanoparticles. The influence of geometric effects, such as percolation paths, on the magnetoresistance of granular systems can be studied.

Acknowledgments

TEM and EELS measurements were made on the JEM 2100F at the IMPMC of the university P and M Curie (Paris VI). The authors sincerely acknowledge Dr B Capelle, director of the IMPMC. We thank Mrs R M Défourneau for her assistance in the conductivity measurements. J Varalda thanks the Brazilian agency FAPESP for financial support.

References

[1] Baibich M N, Broto J M, Fert A, Nguyen Van Dau F, Petroff F, Eitenne P, Creuzet G, Friederich A and Chazelas J 1988 *Phys. Rev. Lett.* **61** 2472–5
[2] Berkowitz A E, Mitchell J R, Carey M J, Young A P, Zhang S, Spada F E, Parker F T, Hutten A and Thomas G 1992 *Phys. Rev. Lett.* **68** 3745–8
[3] Xiao J Q, Samuel Jiang J and Chien C L 1992 *Phys. Rev.* B **46** 9266–9
[4] Rubinstein M 1994 *Phys. Rev.* B **50** 3830–8
[5] Chen T Y, Huang S X, Chien C L and Stiles M D 2006 *Phys. Rev. Lett.* **96** 207203
[6] Serrano-Guisan S, Di Domenicantonio G, Abid M, Abid J-P, Hillenkamp M, Gravier L, Ansermet J-P and Félix C 2006 *Nat. Mater.* **5** 730–4
[7] Fujimori H, Mitani S and Ohnuma S 1995 *Mater. Sci. Eng.* B **31** 219–23
[8] Milner A, Gerber A, Groisman B, Karpovsky M and Gladkikh A 1996 *Phys. Rev. Lett.* **76** 475–8
[9] Peng D L, Sumiyama K, Konno T J, Hihara T and Yamamuro S 1999 *Phys. Rev.* B **60** 2093–100
[10] Holdenried M and Micklitz H 2000 *Eur. Phys. J.* B **13** 205–8
[11] Hattink B J, Garcia del Muro M, Konstantinovic Z, Batlle X, Labarta A and Varela M 2006 *Phys. Rev.* B **73** 045418
[12] Gittleman J I, Goldstein Y and Bozowski S 1972 *Phys. Rev.* B **5** 3609–21
[13] Barzilai S, Goldstein Y, Balberg I and Helman J S 1981 *Phys. Rev.* B **23** 1809–17
[14] Helman J S and Abeles B 1976 *Phys. Rev. Lett.* **37** 1429–32
[15] Inoue J and Maekawa S 1996 Theory of tunnelling magnetoresistance in granular magnetic films *Phys. Rev.* B **53** R11927–9
[16] Mitani S, Takahashi S, Takanashi K, Yakushiji K, Maekawa S and Fujimori H 1998 *Phys. Rev. Lett.* **81** 2799–802
[17] Varalda J, Vodungbo B, Zheng Y, Marangolo M, Ortiz W A, Demaille D, Georges J-M, de Oliveira A J A and Mosca D H 2007 Current-induced magnetization reversal in Co nanoparticles embedded in TiO_2 *Phys. Rev. Lett.* submitted
[18] Varalda J, Ortiz W A, de Oliveira A J A, Vodungbo B, Zheng Y, Demaille D, Marangolo M and Mosca D H 2007 *J. Appl. Phys.* **101** 014318
[19] Guinea F 1998 *Phys. Rev.* B **58** 9212–6
[20] Ohnuma M, Hono K, Abe E, Onodera H, Mitani S and Fujimori H 1997 *J. Appl. Phys.* **82** 5646–52
[21] Ge S, Chi J and Zhang Z 2001 *J. Phys. D: Appl. Phys.* **34** 167–73
[22] Matsumoto Y, Murakami M, Shono T, Hasegawa T, Fukumura T, Kawasaki M, Ahmet P, Chikyow T, Koshihara S and Koinuma H 2001 *Science* **291** 854–6
[23] Wang Z L, Yin J S and Jiang Y D 2000 *Micron* **31** 571–80
[24] Waldner P and Eriksson G 1999 *Calphad* **23** 189–218
[25] Potapov P L, Jorissen K, Schryvers D and Lamoen D 2004 *Phys. Rev.* B **70** 045106
[26] Toyoda T, Nakanishi H, Endo S and Irie T 1985 *J. Phys. D: Appl. Phys.* **18** 747–51
[27] Pascual J, Camassel J and Mathieu H 1978 *Phys. Rev.* B **18** 5606–14
[28] Tang H, Berger H, Schmid P E, Lévy F and Burri G 1993 *Solid State Commun.* **87** 847–50
[29] Grant F A 1959 *Rev. Mod. Phys.* **31** 646–74